Title

Development of a Soluble KIT Electrochemical Aptasensor for Cancer Theranostics

Journal

ACS Sensors, 6(5)

ISSN

2379-3694

Authors

Chung, Saeromi

Sicklick, Jason K

Ray, Partha

et al.

Publication Date

2021-05-28

DOI

10.1021/acssensors.1c00535

Peer reviewed

HHS Public Access

Author manuscript

ACS Sens. Author manuscript; available in PMC 2022 May 28.

Published in final edited form as:

ACS Sens. 2021 May 28; 6(5): 1971–1979. doi:10.1021/acssensors.1c00535.

Development of a Soluble KIT Electrochemical Aptasensor for Cancer Theranostics

Saeromi Chung,

Department of Electrical and Computer Engineering, University of California San Diego, La Jolla, California 92093, United States

Jason K. Sicklick,

Department of Surgery, Division of Surgical Oncology, Moores Cancer Center, University of California San Diego Health, San Diego, California 92093, United States

Partha Ray,

Department of Surgery, Division of Surgical Oncology, Moores Cancer Center, University of California San Diego Health, San Diego, California 92093, United States;

Drew A. Hall

Department of Electrical and Computer Engineering and Department of Bioengineering, University of California San Diego, La Jolla, California 92093, United States;

Abstract

An electrochemical sensor based on a conformation-changing aptamer is reported to detect soluble KIT, a cancer biomarker, in human serum. The sensor was fabricated with a ferrocene-labeled aptamer (K_d < 5 nM) conjugated to a gold electrode. Quantitative KIT detection was achieved using electrochemical impedance spectroscopy (EIS) and square-wave voltammetry (SWV). EIS was used to optimize experimental parameters such as the aptamer-to-spacer ratio, aptamer immobilization time, pH, and KIT incubation time, and the sensor surface was characterized using voltammetry. The assay specificity was demonstrated using interfering species and exhibited high specificity toward the target protein. The aptasensor showed a wide dynamic range, 10 pg/mL–100 ng/mL in buffer, with a 1.15 pg/mL limit of detection. The sensor also has a linear response to KIT spiked in human serum and successfully detected KIT in cancer-cell-conditioned media. The proposed aptasensor has applications as a continuous or intermittent approach for cancer therapy monitoring and diagnostics (theranostics).

Graphical Abstract

Corresponding Authors: Partha Ray – Department of Surgery, Division of Surgical Oncology, Moores Cancer Center, University of California San Diego Health, San Diego, California 92093, United States; pray@health.ucsd.edu, **Drew A. Hall** – Department of Electrical and Computer Engineering and Department of Bioengineering, University of California San Diego, La Jolla, California 92093, United States; drewhall@ucsd.edu.

Supporting Information

The Supporting Information is available free of charge at https://pubs.acs.org/doi/10.1021/acssensors.1c00535.

CD spectroscopy results; optimization of experimental parameters; reproducibility study; KIT detection in human serum; serum stability; temperature stability; and KIT detection in cell media (PDF)

Complete contact information is available at: https://pubs.acs.org/10.1021/acssensors.1c00535

The authors declare no competing financial interest.

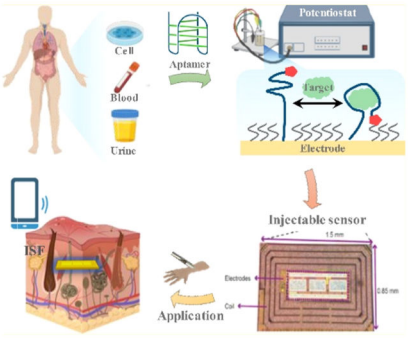

Keywords

KIT; aptamer; electrochemical sensor; cancer; square-wave voltammetry; aptasensor; theranostics

Cancer is a noncommunicable disease responsible for most global deaths. Worldwide, one out of six deaths is attributed to cancer—more than the mortality caused by tuberculosis, HIV/AIDS, and malaria combined. In 2018, there were ~17 million new cancer cases diagnosed worldwide, causing 9.5 million deaths.[1] In the 21st century, cancer is the single most significant barrier toward increasing life expectancy. Critically, many cancers are diagnosed at an advanced stage when treatments are limited, resulting in a persistently high mortality rate. Notably, several serum cancer biomarkers have been identified, such as CA-125 for ovarian cancer,[2] CA 19.9 for pancreatic cancer,[3] S100 for Melanoma,[4] carcinoembryonic antigen for colorectal cancer,[5] alpha-fetoprotein for hepatocellular carcinoma,[6] and prostate-specific antigen for prostate cancer.[7] Cancer detection and treatment monitoring through biomarkers that can be measured at the point-of-care (POC), especially in low resource settings, could significantly reduce cancer-related morbidity and mortality and increase the overall survival rate of patients.[8]

In this regard, the KIT protein's prognostic significance in cancer patients has received intense interest.[9–12] c-KIT, also a known proto-oncogene, is a receptor tyrosine kinase that, upon binding to its ligand, stem cell factor, dimerizes and initiates a cascade of signal transduction that regulates cell growth and proliferation. Overexpression or mutations in functionally important domains of the gene are associated with cancers, including gastrointestinal stromal tumor (GIST),[10–12] mast cell disease (systemic mastocytosis), acute myeloid leukemia, testicular seminoma, and melanoma.[13] In health and disease, the ligand-binding extracellular portion of the c-KIT protein is cleaved from the cell surface by the metalloprotease, tumor necrosis factor α-converting enzyme (TACE or ADAM-17), and generates a soluble KIT (sKIT) fragment.[14,15] The resulting product, sKIT, can be detected in the serum or plasma of patients with various pathological conditions and functions as a biomarker of cancer.[11,16–19]

Full-length c-KIT and sKIT have been studied as a biomarker with various detection methods, including flow cytometry,[20,21] immunohistochemical analysis,[22] and enzyme-linked immunosorbent assay (ELISA).[18] Although these methods provide quantitative information, they require complicated pretreatment steps, large sample volume, expensive

laboratory reagents, and sophisticated instruments, which preclude POC operation.[24,25] On the other hand, electrochemical detection techniques enable rapid, robust, simple, and sensitive monitoring of the interaction between a target protein and the sensor surface modified with its receptor or ligand molecule.[23–25] Thus, electrochemical biosensors can be used to diagnose and monitor cancers and provide a prognostic approach to the treatment. However, there are no reports of an electrochemical biosensor for the detection of sKIT.

Recently, electrochemical aptamer-based sensors, “aptasensors”, have drawn significant interest.[26,27] Aptamers are single-stranded DNA or RNA oligonucleotides selected by an *in vitro* iterative process known as systematic evolution of ligands by exponential enrichment.[28,29] The nucleotides in the single-stranded aptamer molecules undergo intramolecular Watson–Crick base pairing to initially form secondary and subsequently tertiary structures to assume three-dimensional shapes that function as ligands that bind to their cognate proteins with high binding affinity and specificity, which is analogous to monoclonal antibodies.[30–32] This conformation-changing property of the aptamer structure upon protein binding has been utilized in biosensors where a redox-active molecule is covalently conjugated to the aptamer immobilized on an electrode surface.[33–35] The binding of the cognate protein to the aptamer changes its conformation and thus the redox probe’s distance from the electrode.[36–39] This, in turn, alters the electron-transfer profile between the redox molecule and the electrode. Thus, the aptamer–protein binding event is transduced into an electronic signal that quantifies the amount of protein present in a sample.[35,40]

In this work, we used a DNA aptamer against c-KIT with high affinity and specificity (K_d < 5 nM).[20,41] The aptamer was covalently conjugated to a ferrocene (Fc) redox label and immobilized on a gold electrode to form a novel electrochemical aptasensor, as shown in Figure 1. The resulting aptasensor based on a thin gold-film electrode offers high electrical conductivity, biocompatibility, and good chemical stability in biofluids along with mass production, cost controllability, and high sensitivity. The aptasensor was read out using square-wave voltammetry to detect sKIT in the conditioned media of cancer cell lines for the first time to show its clinical applicability. This target-induced conformational change of the aptamer-based sensor has the potential to be used as a diagnostic tool to evaluate the biomarker present in the biological fluids. Such an assay could be further coupled with injectable sensors (Figure 1A) or wearable sensors for continuous monitoring of KIT levels in response to therapy, closing the personalized medicine cancer treatment loop.[42] Thus, the aptasensor can function as both a diagnostic and therapeutic response tool, hence the name *theranostics*.

MATERIALS AND METHODS

Reagents and Instruments.

Magnesium chloride ($MgCl_2$; #208337), phosphate-buffered saline (PBS; #P5493), Tris[2-carboxyethyl] phosphine (TCEP; #C4706), 6-mercapto-1-hexanol (#725226), β-mercaptoethanol (#M6250), *N*-hydroxysuccinimide (NHS; #130672), ferrocene carboxylic acid (Fc; #106887), human serum albumin (HSA; #A9511–100MG), fibrinogen (FBG; #341576–100MG), 1,4-dithiothreitol (DTT; #233156), Dulbecco’s modified Eagles medium (DMEM; #D6429–500ML), fetal bovine serum (FBS; F2442–500ML), Iscove’s modified

Dulbecco's medium (IMDM; 51471C-1000ML), radioimmunoprecipitation assay buffer (RIPA; R0278–50ML), and 1-thioglycerol (#M6145–25ML) were purchased from Sigma-Aldrich. Human AB serum (#01024) was bought from Omega Scientific, and Ulex europaeus agglutinin I (UEA; #L-1060) was purchased from Vector Laboratories. Fetal bovine serum (FBS; # A31604), penicillin/streptomycin (#15140122), and Pierce protease and phosphatase inhibitor (#A32959) were purchased from Thermo Fisher Scientific. Interleukin 6 (IL-6; #206-IL) was purchased from R&D Systems and *N*-ethyl-*N*′-(3-dimethyl aminopropyl) carbodiimide hydrochloride (EDC; #BC25–5) from G-Biosciences. Purified c-KIT protein containing the extracellular domain (Met 1-Thr 516) with a polyhistidine tag at the C-terminus (#11996-H08H) was purchased from Sino Biological. The primary mouse monoclonal anti-KIT antibody (#3308) was obtained from Cell Signaling Technology and the secondary, horseradish peroxidase-conjugated antimouse IgG (#31430) from Invitrogen. Immun-Blot PVDF membrane (#1620177) and prestained molecular weight marker (#1610375) were acquired from Bio-Rad.

The single-stranded DNA KIT aptamer (5′-GAG GCA TAC CAG CTT ATT CAA GGG GCC GGG GCA AGG GGG GGG TAC CGT GGT AGG ACA TAG TAA GTG CAA TCT GCG AA-3′) and the scrambled control oligo (5′-TGA CGG GAG ACT TAA AAC GCA AGG GGT GCA GCT ATC GCG GAG GCC AAG GGT TCA AGT CGA CGG GTA GCT AGG TTG GA-3′) were synthesized with 5′-S-S- (disulfide bond) and 3′-NH_2 (amine group) modifications by Integrated DNA Technologies. We obtained the GIST-T1 cell line from T. Taguchi (Kochi Medical School, Japan), the human mast cell line HMC 1.2 from I. Pass (Sanford Burnham Prebys Medical Discovery Institute, San Diego), and the pancreatic cancer cell line MiaPaCa-2 from ATCC.[20]

Square-wave voltammetry (SWV), cyclic voltammetry (CV), and electrochemical impedance spectroscopy (EIS) measurements were performed using a benchtop potentiostat (CH Instruments, 750E). A three-electrode setup was used for all experiments with Au, Ag/AgCl, and Pt wire (CH Instruments, #CHI115) as the working electrode (WE), reference electrode (RE), and counter electrode (CE), respectively.

KIT Aptasensor Fabrication.

Gold-coated microscope slides (100 nm thickness, 99.999% Au film purity on a 5 nm Cr adhesion layer) were used as the WE (5 mm diameter). Each WE ($6.25 \times 10^{-6} m^2$ area) was sectionalized by a nonconductive (Teflon) custom-made electrode holder with wells that hold up to 100 μL. This fixture maintains the electrode area during the surface modification and measurements. Before electrode modification, the WE was chemically treated with a mixture of H_2SO_4 and H_2O_2, followed by washing with distilled water. It was then electrochemically cleaned by potential cycling from 0 to 1.4 V versus Ag/AgCl in 0.1 M H_2SO_4. The thiolated aptamer was activated with TCEP for 2 h at room temperature. The WE was functionalized by immersing it in a solution containing 0.5 μM aptamer in 500 μL of incubation buffer [5 mM $MgCl_2$, 0.5 mM DTT in 20 mM PBS (pH 7.4)] with 0.5 μM 6-mercapto-1-hexanol on a shaking incubator (Thermo Scientific, #4625) at room temperature for 12 h. The WE was then gently rinsed with distilled water and equilibrated with the incubation buffer for 30 min on a shaking incubator. To remove the unbound

aptamer and block the surface, the electrode was incubated in 10 mM β-mercaptoethanol for 30 min at room temperature. Last, the amine-terminated aptamers were modified with Fc by EDC/NHS coupling. 15 mg of ferrocene carboxylic acid was dissolved in 1 mL of absolute ethanol, and 11.5 mg of NHS and 76.7 mg of EDC were dissolved in 1 mL of PBS (pH 5.0). The mixture containing 15 μL of 64 mM ferrocene carboxylic acid and 985 μL of EDC/NHS solution was prepared so that the reagents' concentration was 1, 100, and 400 mM ferrocene carboxylic acid, NHS, and EDC, respectively. After that, 50 μL of the activated solution was drop-cast onto the aptamer-modified electrode and kept overnight at room temperature.[43] In this step, a carbodiimide bond forms between the activated carboxylic groups of ferrocene carboxylic acid and the amino-labeled aptamers. The stepwise assembly was monitored using CV and EIS with 5 mM $[Fe(CN)_6]^{4-/3-}$ in 0.1 M PBS and SWV in 0.1 M PBS. All prepared electrodes were inspected in the buffer solution at every step during the immobilization process to select the ones having a similar response for the quantitative measurement of KIT.

Atomic Force Microscopy Surface Characterization.

The surface morphology was investigated using a Veeco Scanning Probe Microscope with a Nanoscope IV controller (Veeco Instruments, Woodbury, NY, USA) in the tapping mode. 5 mm × 5 mm gold-coated slides were used as probes. Images were obtained in air at room temperature and controlled humidity. The images were analyzed by Veeco Instruments software.

Circular Dichroism Spectroscopy.

Circular dichroism (CD) experiments were performed with a CD Spectrometer (Aviv Instruments, model 202) and a quartz cuvette with a 1 mm optical path length. 400 μL of the KIT aptamer (10 μM) in 100 mM potassium phosphate buffer (pH 7.1) was loaded in the cuvette, and spectra were recorded in the wavelengths of 220–320 nm in 1 nm steps at 25 °C. All scans were done in triplicate, and the average of the buffer CD (baseline) was subtracted from all other measurements.

KIT Assays.

Calibration curves were generated by incubating the KIT aptasensor with various KIT concentrations (10 pg/mL–100 ng/mL) in 0.1 M PBS for 30 min at room temperature and measured with SWV and EIS. Control assays to look at nonspecific binding were performed with the control (scrambled) oligo-modified sensor incubated with 10 pg/mL KIT. Selectivity was assessed using 1.0 μg/mL IL-6, UEA I, BSA, FBG, or HSA incubated for 30 min at room temperature in 0.1 M PBS (pH 7.4) and then measured using SWV and EIS. Voltammograms were recorded using SWV (−150 to +450 mV at 50 mV/s) in 0.1 M PBS (pH 7.4). EIS measurements (10 Hz to 100 kHz with a 5 mV ac amplitude) were performed with 5 mM $[Fe(CN_6)]^{4-/3-}$ in 0.1 M PBS.

Cell Culturing.

GIST-T1 cells were grown in DMEM with 10% FBS, 1% penicillin/streptomycin, and 2 mM glutamine.[44] The human mast cell line HMC-1.2 was cultured in IMDM with 10% FBS,

1% penicillin/streptomycin, and 1.2 mM 1-thioglycerol.[20] GIST-T1 is an adherent cell line, and HMC 1.2 cells grow in suspension. The growth medium was collected and centrifuged at 1000 rpm and 4 °C to remove suspended cells (HMC-1.2) and nonadherent dead cells (GIST-T1). The resulting supernatant was collected and centrifuged at 13,000 rpm and 4 °C to remove residual cellular debris. The supernatant (conditioned media, CM) was collected and stored in aliquots at −80 °C. The CM was used to estimate the soluble sKIT using ELISA (Human CD117/c-kit Immunoassay; R&D Systems, Inc. #DSCR00).

Cell Culture Assays.

For western blot, GIST-T1 cells were homogenized in the RIPA buffer. 30 μL of the conditioned media and 5 μL of the GIST-cell lysate were loaded and separated by sodium dodecyl sulfate–polyacrylamide gel electrophoresis before transfer to a nitrocellulose membrane. Membranes were incubated with a primary anti-KIT antibody (1:1000). A secondary antibody, horseradish peroxidase-conjugated anti-mouse IgG (1:5000), was added, and antibody complexes were detected by an enhanced chemiluminescence (ECL) system (Thermo Fisher Scientific, #32109). A prestained molecular weight marker was run in parallel to determine the molecular weight of the proteins. For electrochemical detection, sKIT-containing supernatant obtained by centrifuging the growth medium was diluted to the appropriate concentration, incubated with the aptasensor for 30 min, and recorded using SWV.

Statistical Analysis.

All data were obtained from a minimum of three independent experiments, and error bars represent one standard deviation (SD). Statistical analysis was performed with Origin 9.0. The limit of detection (LOD) was calculated using LOD = 3 × SD of blank (95% confidence level).

RESULTS AND DISCUSSION

Guanine (G) nucleotide-rich DNA and RNA aptamers can form a four-stranded helical structure called a G-quadruplex. Four guanines connect to form a square-planar structure called the guanine tetrad through the cyclic Hoogsteen hydrogen bonding. Two or more of these guanine tetrad layers stack to form a G-quadruplex structure. These intricate structural motifs are thermodynamically stable and resistant to many serum nucleases that make them desirable candidates as therapeutic and diagnostic agents for cancer treatment.[45,46] The G-quadruplex aptamers also undergo a structural change in the conformation upon ligand binding and are especially suited for electrochemical aptasensor fabrication.[47,48]

The conformation-changing aptasensor concept is illustrated in Figure 1B. The sensor is functionalized with a mixture of aptamer and spacer molecules that bind to the gold electrode surface via a self-assembled chemisorption reaction between sulfur and Au, forming Au–S bonds.[49] In the absence of the target molecule (KIT protein in this work), the aptamer tagged with a Fc reporter is in a semiopen conformation where the reporter is away from the sensor surface, as shown in Figure 1C. Upon binding to KIT, the aptamer switches to a rigid, target-specific G-quadruplex structure that brings the reporter near the

electrode surface. Modulating the reporter position results in a decreased electron-transfer rate between Fc and the electrode that is read out using voltammetry techniques.

Aptasensor Surface Characterization.

Each step in the aptasensor fabrication was characterized by EIS and CV starting with the unlabeled KIT aptamer (Au/aptamer). EIS was used to measure the charge-transfer resistance, R_{ct}, whereas CV measured the peak current. Spectra for a bare Au electrode, Au/aptamer, and Au/aptamer/KIT with various KIT concentrations ranging from 10 pg/mL to 10 ng/mL are shown in Figure 2A. The formation of the aptamer–protein complex disrupted the electron transfer between the ferri/ferrocyanide solution $\{[Fe(CN_6)]^{4-/3-}\}$ and the sensor surface, leading to an increase in R_{ct}. The measured Nyquist plots show an R_{ct} increase after the aptamer immobilization (Au/aptamer) from 5.07 to 8.91 kΩ. After incubating with the KIT protein, the change in R_{ct} [$\Delta R_{ct} = R_{ct}(\text{KIT}) - R_{ct}$ (blank)] linearly increased for KIT concentrations from 10 pg/mL to 10 ng/mL.

Figure 2B shows the linear relationship between KIT concentration and ΔR_{ct}, demonstrating that the KIT protein interacted with the aptamer. Control experiments using the KIT aptamer (Au/aptamer) and a scrambled version of the aptamer (Au/control) further proved this. The control sensor did not show a significant ΔR_{ct} (0.43 ± 0.25 kΩ), thus indicating no binding compared to the KIT sensor (5.74 ± 0.36 kΩ), which had significant binding, as shown in Figure 2C. CV measurements were also performed to assess the sensor performance. As shown in Figure 2D, the voltammograms have well-defined redox peaks for $[Fe(CN_6)]^{4-/3-}$. The aptamer-modified sensor (Au/aptamer) showed a lower peak current due to the aptamer immobilization, resulting in an R_{ct} increase. After incubation with 10 and 100 pg/mL KIT, the current responses decreased further because the KIT–aptamer complex blocked the electron-transfer process between the solution and the electrode. We also characterized the surface with atomic force microscopy (AFM). The topographic images of (i) Au, (ii) Au/Apt, (iii) Au/Apt-Fc, and (iv) Au/Apt-Fc/KIT surfaces are shown in Figure 2E and suggest structural differences between the layers. The bare gold layer was the smoothest (<10 nm variation), whereas after aptamer immobilization (ii–iii), the surface morphology exhibited increased, homogeneous surface roughness. The interaction of the KIT protein with the sensing layer gave rise to globular structures (iv). The AFM data are consistent with the electrochemical data. Together, these data demonstrate that the KIT aptamer is selective toward the target molecule and that the sensor is well assembled.

To characterize the secondary aptamer structure, CD analysis was performed in 0.1 M PBS. Figure S1A shows that the CD spectra have a negative peak at 245 nm and a positive peak at 270 nm, which is the inherent DNA characteristic of the G-quadruplex structure due to the multiple π–π^* transitions.[50] Chronoamperometry was used to confirm the electron-transfer rate difference between the unbound and KIT-bound aptamer (Figure S1B). We observed a shorter exponential Faradaic current decay time with KIT compared to that without the KIT protein. These results demonstrate that the aptamer conformational change affects the electron-transfer kinetics.

Aptasensor Optimization.

After demonstrating the concept's viability, we optimized the parameters (i.e., aptamer-to-spacer ratio, aptamer immobilization time, pH, and KIT incubation time) to obtain the best sensor response. It is well known that the aptamer-to-spacer (6-mercapto-1-hexanol) ratio in conformation-changing assays affects the performance as the spacer provides room to form the aptamer–protein complex. Aptamer and spacer ratios from 1:0 to 1:50 were investigated at a fixed KIT concentration (10 ng/mL). The measured ΔR_{ct} monotonically increased from a 1:0 to a 1:1 ratio and then declined (Figure S2A). From these data, the 1:1 ratio was chosen for all subsequent experiments. Next, the aptamer incubation time was studied by incubating 0.5 μM aptamer on the electrode from 1 to 24 h. ΔR_{ct} consistently increased from 1 to 12 h and then plateaued, indicating that the sensor surface was saturated by the aptamer and spacer molecules (Figure S2B). The effect of pH was examined over the range of 6.0–8.0 (Figure S2C). The response increased gradually from 6.0 to 7.4, whereas it rapidly decreased at a higher pH, likely due to the protein stability. The optimum pH for all subsequent experiments was selected to be 7.4, similar to physiological biofluid levels. Last, the effect of the target incubation time was studied, ranging from 5 to 40 min, as shown in Figure S2D. In our envisioned *in vivo* application for treatment monitoring, this does not apply, but we did so for completeness. In these experiments, ΔR_{ct} monotonically increased up to 30 min incubation and then plateaued. From these results, the optimized conditions were a 1:1 ratio of the aptamer to the spacer, 12 h aptamer immobilization, an assay pH of 7.4, and a 30 min sample incubation time. These values were used for all subsequent experiments.

Ferrocene Reporter.

The assay described thus far used a traditional route with a redox couple in the buffer, ferri-/ferrocyanide. To remove the need for a redox couple toward "reagentless" *in vivo* monitoring, we modified the amine terminus of the aptamer with a redox reporter, Fc. The electrochemical behavior of each step in the fabrication process was investigated using SWV in PBS with the optimized parameters previously described, as shown in Figure 3. Voltammograms were recorded for both the KIT aptamer and a scrambled version as a negative control. The ferrocene oxidation peak is visible at 123 mV for Au/Fc-Apt due to the electrochemical signal of Fc, whereas it was not observed for the bare Au, Au/spacer, or Au/aptamer modification steps. As expected, after incubating with 100 pg/mL KIT, the Au/Fc-Apt-modified electrode had an increased peak current (0.668 μA) compared to without KIT (0.262 μA) due to the conformation change of the aptamer modulating the location of the Fc reporter (Figure 3A). The scrambled control oligonucleotide was tested in the same manner. As shown in Figure 3B, the voltammograms without the Fc reporter (i.e., Au/control and Au/control/KIT) did not exhibit an appreciable current response. After labeling the control oligo with the Fc reporter (Au/Fc-control), the Fc oxidation peak at 128 mV was present but did not increase after incubation with 100 pg/mL KIT, indicating that the control oligo is not binding to KIT. These results provide further evidence that the aptamer conformation change is specific to KIT and that the aptasensor can be read out using the Fc reporter and SWV.

KIT Detection Using a Conformation-Changing Aptasensor.

To assess the assay performance, KIT was incubated on the sensor with concentrations ranging from 10 pg/mL to 100 ng/mL and measured using SWV in PBS (pH = 7.4). In the presence of KIT, the Fc oxidation peak increased compared to the blank solution due to the direct electron transfer of Fc resulting from the aptamer conformation change. As shown in Figure 3C, the current response increased proportionally with the KIT concentration. These data were compiled into a calibration curve (Figure 3D) showing the linear relationship. The assay has a 1.15 pg/mL LOD and a limit of quantification (LOQ) of 10.0 pg/mL with a linear dynamic range from 10 pg/mL to 100 ng/mL. The sensor reproducibility was evaluated by measuring 0.5 ng/mL KIT with five independent electrodes. The coefficient of variation was 2.35%, indicating that the proposed sensor exhibited high reproducibility (Figure S3). The coefficient of variation is comparable to previously reported methods for KIT detection [2.2–9.4% for ELISA,[51,52] 0.04–34.0% of multiplex immune-polymerase chain reaction (mI-PCR)].[53]

Selectivity.

Selectivity is an important characteristic of any receptor-target-based assay. While the specificity of the KIT aptamer was previously reported,[20,41] it is crucial to verify the specificity with the Fc reporter's addition and the change to electrochemical rather than optical readout. To investigate the selectivity of the conformation-changing aptasensor, voltammograms with various off-target proteins (IL-6, UEA, BSA, FBG, and HSA) were measured, as shown in Figure 4A. In all cases, the interfering protein's current responses were significantly lower than 0.1 μg/mL KIT, despite being present at an order of magnitude higher concentration, indicating that the proposed sensor has good selectivity. Next, the aptasensor was examined in human serum spiked with KIT toward an *in vivo* application. The serum was diluted 10-fold with PBS to mimic interstitial fluid (ISF), and KIT was spiked in at concentrations of 10 pg/mL, 500 pg/mL, and 100 ng/mL. Figure 4B shows the measured voltammograms where the current response increased linearly proportional to the KIT concentration. The corresponding calibration curve is shown in Figure 4C, confirming the linear relationship. The different slopes of the calibration curves in buffer (0.252 ± 0.005) and 10% serum (0.231 ± 0.024) were likely due to matrix effects. The serum response was slightly reduced; however, it revealed no significant differences between the two slopes in the calibration curves (<6.15% of RSD). These data demonstrate that the KIT aptasensor has applicability in clinically relevant biofluids with high levels of background-interfering species.

Cell Culture Media and Serum Assays.

KIT is known to be overexpressed in GIST and Mastocytosis.[20] It has been shown that a sKIT fragment is released from cell surfaces and can be used for cancer theranostics.[10–12] To investigate the clinical applicability of the reported KIT conformation-changing aptasensor toward *in vivo* cancer treatment monitoring, we collected conditioned media containing sKIT from a GIST (GIST-T1) and a Systemic Mastocytosis (HMC-1.2) cell line, each of which has an oncogenic KIT mutation and overexpresses the KIT protein.[54,55] Conditioned media from a pancreatic cancer cell line, MIA-PaCa2, which does

not express KIT, were used as a control. Each supernatant was diluted 10^4-fold in PBS solution and incubated on the aptasensor for 30 min (Figure 5A,B). From the triplicate measurements, KIT concentrations were determined to be 12.84 ± 3.99 and 7.08 ± 1.98 ng/mL for HMC-1.2 and GIST-T1, respectively, whereas it was 0.06 ± 0.04 ng/mL for MIA-PaCa2 (Figure 5C). These data are consistent with the western blot results run on the same samples (Figure 5D).[20] With electrochemical and western blot measurements, sKIT concentrations in the conditioned media of HMC-1.2 and GIST-T1 cells, which overexpress KIT, were significantly higher than that in MIA-PaCa2 cells. We also tested the aptasensor performance using three independent sensors on 3 different days with a commercially available ELISA kit, where the three independent samples were analyzed. The results of the CM (background subtracted) for HMC-1.2, GIST-T1, and MIA-PaCa2 cells were 6.36 ± 0.28, 3.28 ± 0.55, and 0.03 ± 0.02 ng/mL, respectively. The measurements between different cell lines were similar; however, the sKIT levels detected using the aptasensor were higher than that of ELISA, possibly due to the higher affinity and sensitivity of the reagent (receptor)[59] and different sensing approaches.[60] To investigate the recovery of the KIT aptasensor, known KIT concentrations (0.1, 1, and 10 ng/mL) were spiked into the ISF mimic (10× diluted human serum). The percent recovery of spiked samples ranged from 85.9 to 117.5% (Table S1 and Figure S4). These measurements demonstrate that the developed conformation-changing aptasensor has high selectivity and sensitivity to KIT in physiologically relevant biofluids.

Toward the *in vivo* application of this assay, the aptasensor stability in serum and the temperature dependence were assessed. The sensor was stable for 30 min without any signal loss but lost half of the signal after 4 h (Figure S5). The aptamer's backbone should be chemically modified to improve the sensor stability and reliance against deoxyribonucleases and will be the focus of future work. The temperature stability was investigated by incubating a fixed concentration of KIT and varying the temperature from 7 to 55 °C (Figure S6). Interestingly, the signal was the highest at 7 °C, decreased slightly from 14 to 37 °C, and then significantly decreased at higher temperatures, likely due to the aptamer and/or KIT protein denaturation. The temperature range is compatible with the human body, pointing toward the implanted therapy monitor application.

Comparison.

KIT is detected using ELISA, immunohistochemical, western blot, flow cytometry, and mI-PCR techniques. The analytical performances of these are summarized in Table 1. The proposed electrochemical aptasensor has the widest linear range and the best LOD. The proposed sensor has an 80× lower LOD and 2 decades broader dynamic range than a commercial ELISA kit, the current gold standard for clinical detection.[51] Importantly, the aptasensor's dynamic range covers the physiological range of sKIT in serum, indicating the clinical applicability to biofluids such as ISF for continuous monitoring.[61] The proposed technique is capable of both *in vitro* and *in vivo* monitoring, uniquely positioning it for diagnostic and therapeutic applications, hence the "theranostic" designation.

CONCLUSIONS

A novel electrochemical conformation-changing aptasensor with a ferrocene reporter toward a GIST cancer biomarker, KIT, was developed to study the clinical applicability in this work. The stepwise sensor modification was investigated using CV and EIS, and experimental parameters such as the spacer ratio, aptamer immobilization time, pH, and KIT incubation time were optimized. In PBS, the aptasensor has a 1.15 pg/mL LOD and a 10 pg/mL–100 ng/mL linear dynamic range. The sensor was tested with off-target, interfering species and supernatant of the conditioned medium with no appreciable nonspecific binding. The proposed sensor could detect the sKIT within 35 min, unlike the traditional ELISA technique requiring several hours. The sensor successfully detected the sKIT released from the HMC-1.2 and GIST-T1 cells, which demonstrates that the reported aptasensor has high specificity and high sensitivity. Therefore, the developed method can be applied as a fast routine laboratory test in CM, serum, and plasma samples obtained from clinical laboratories. Furthermore, this work lays the foundation for a reagentless assay toward the *in vivo* treatment monitoring of KIT-overexpressing cancers.

Supplementary Material

Refer to Web version on PubMed Central for supplementary material.

ACKNOWLEDGMENTS

This work was partially supported by the National Science Foundation (1621825), the National Institutes of Health (R41DA044905, R01 CA226803, and UL1TR001442), the UCSD Center for Wearable Systems (CWS), Samsung, the Food and Drug Administration (R01 FD006334), and the GIST Research Fund. The content is solely the responsibility of the author(s) and does not necessarily represent the official views of the National Institutes of Health. The authors thank Dr. Sumeet Handa for help with CD spectroscopy measurements and Dr. Ryan Nicholl for help with AFM measurements.

REFERENCES

(1). Bray F; Ferlay J; Soerjomataram I; Siegel RL; Torre LA; Jemal A Global Cancer Statistics 2018: GLOBOCAN Estimates of Incidence and Mortality Worldwide for 36 Cancers in 185 Countries. Ca-Cancer J. Clin 2018, 68, 394–424. [PubMed: 30207593]

(2). Scholler N; Urban N CA125 in Ovarian Cancer. Biomarkers Med. 2007, 1, 513–523.

(3). Poruk KE; Gay DZ; Brown K; Mulvihill JD; Boucher KM; Scaife CL; Firpo MA; Mulvihill SJ The Clinical Utility of CA 19–9 in Pancreatic Adenocarcinoma: Diagnostic and Prognostic Updates. Curr. Mol. Med 2013, 13, 340–351. [PubMed: 23331006]

(4). Harpio R; Einarsson R S100 Proteins as Cancer Biomarkers with Focus on S100B in Malignant Melanoma. Clin. Biochem 2004, 37, 512–518. [PubMed: 15234232]

(5). Nicholson BD; Shinkins B; Pathiraja I; Roberts NW; James TJ; Mallett S; Perera R; Primrose JN; Mant D Blood CEA Levels for Detecting Recurrent Colorectal Cancer. Cochrane Database Syst. Rev 2015, 12, CD011134.

(6). Arrieta O; Cacho B; Morales-Espinosa D; Ruelas-Villavicencio A; Flores-Estrada D; Hernández-Pedro N The Progressive Elevation of Alpha Fetoprotein for the Diagnosis of Hepatocellular Carcinoma in Patients with Liver Cirrhosis. BMC Canc. 2007, 7, 28.

(7). Reverri E; Devitt A; Kajzer J; Baggs G; Borschel M Review of the Clinical Experiences of Feeding Infants Formula Containing the Human Milk Oligosaccharide 2′-Fucosyllactose. Nutrients 2018, 10, 1346.

(8). Goossens N; Nakagawa S; Sun X; Hoshida Y Cancer Biomarker Discovery and Validation. Transl. Cancer Res 2015, 4, 256–269. [PubMed: 26213686]

(9). Hristova VA; Chan DW Cancer Biomarker Discovery and Translation: Proteomics and Beyond. Expert Rev. Proteomics 2019, 16, 93–103. [PubMed: 30556752]

(10). Akin C; Schwartz LB; Kitoh T; Obayashi H; Worobec AS; Scott LM; Metcalfe DD Soluble Stem Cell Factor Receptor (CD117) and IL-2 Receptor Alpha Chain (CD25) Levels in the Plasma of Patients with Mastocytosis: Relationships to Disease Severity and Bone Marrow Pathology. Blood 2000, 96, 1267–1273. [PubMed: 10942367]

(11). DePrimo SE; Huang X; Blackstein ME; Garrett CR; Harmon CS; Schöffski P; Shah MH; Verweij J; Baum CM; Demetri GD Circulating Levels of Soluble KIT Serve as a Biomarker for Clinical Outcome in Gastrointestinal Stromal Tumor Patients Receiving Sunitinib Following Imatinib Failure. Clin. Cancer Res 2009, 15, 5869–5877. [PubMed: 19737953]

(12). Sarlomo-Rikala M; Kovatich AJ; Barusevicius A; Miettinen M CD117: A Sensitive Marker for Gastrointestinal Stromal Tumors That Is More Specific than CD34. Mod. Pathol 1998, 11, 728–734. [PubMed: 9720500]

(13). Miettinen M; Lasota J KIT (CD117): A Review on Expression in Normal and Neoplastic Tissues, and Mutations and Their Clinicopathologic Correlation. Appl. Immunohistochem. Mol. Morphol 2005, 13, 205–220. [PubMed: 16082245]

(14). Black RA Tumor necrosis factor-α converting enzyme. Int. J. Biochem. Cell Biol 2002, 34, 1–5. [PubMed: 11733179]

(15). Wypych J; Bennett L; Schwartz M; Clogston C; Lu H; Broudy V; Bartley T; Parker V; Langley K Soluble Kit Receptor in Human Serum. Blood 1995, 85, 66–73. [PubMed: 7528574]

(16). Kawakita M; Yonemura Y; Miyake H; Ohkubo T; Asou N; Hayakawa K; Nakamura M; Kitoh T; Osawa H; Takatsuki K; Suda T Soluble C-Kit Molecule in Serum from Healthy Individuals and Patients with Haemopoietic Disorders. Br. J. Haematol 1995, 91, 23–29. [PubMed: 7577639]

(17). Makowska JS; Cieslak M; Kowalski ML Stem Cell Factor and Its Soluble Receptor (c-Kit) in Serum of Asthmatic Patients-Correlation with Disease Severity. BMC Pulm. Med 2009, 9, 27. [PubMed: 19480722]

(18). Tajima F; Kawatani T; Ishiga K; Nanba E; Kawasaki H Serum Soluble C-Kit Receptor and Expression of c-Kit Protein and MRNA in Acute Myeloid Leukemia. Eur. J. Haematol 1998, 60, 289–296. [PubMed: 9654158]

(19). Zhong H-L; Lu X-Z; Chen X-M; Yang X-H; Zhang HF; Zhou L; Wang L; Cao K-J; Huang J Relationship between Stem Cell Factor/c-Kit Expression in Peripheral Blood and Blood Pressure. J. Hum. Hypertens 2010, 24, 220–225. [PubMed: 19675587]

(20). Banerjee S; Yoon H; Yebra M; Tang C-M; Gilardi M; Shankara Narayanan JS; White RR; Sicklick JK; Ray P Anti-KIT DNA Aptamer for Targeted Labeling of Gastrointestinal Stromal Tumor. Mol. Cancer Ther 2020, 19, 1173–1182. [PubMed: 32127469]

(21). Naeem M; Dahiya M; Clark JI; Creech SD; Alkan S Analysis of C-Kit Protein Expression in Small-Cell Lung Carcinoma and Its Implication for Prognosis. Hum. Pathol 2002, 33, 1182–1187. [PubMed: 12514786]

(22). Pilloni L; Bianco P; Difelice E; Cabras S; Castellanos ME; Atzori L; Ferreli C; Mulas P; Nemolato S; Faa G The Usefulness of C-Kit in the Immunohistochemical Assessment of Melanocytic Lesions. Eur. J. Histochem 2011, 55, 20.

(23). Moon J-M; Kim D-M; Kim MH; Han J-Y; Jung D-K; Shim Y-B A Disposable Amperometric Dual-Sensor for the Detection of Hemoglobin and Glycated Hemoglobin in a Finger Prick Blood Sample. Biosens. Bioelectron 2017, 91, 128–135. [PubMed: 28006679]

(24). Chung S; Moon J-M; Choi J; Hwang H; Shim Y-B Magnetic Force Assisted Electrochemical Sensor for the Detection of Thrombin with Aptamer-Antibody Sandwich Formation. Biosens. Bioelectron 2018, 117, 480–486. [PubMed: 29982117]

(25). Sun AC; Hall DA Point-of-Care Smartphone-Based Electrochemical Biosensing. Electroanalysis 2019, 31, 2–16.

(26). Lai RY; Plaxco KW; Heeger AJ Aptamer-Based Electrochemical Detection of Picomolar Platelet-Derived Growth Factor Directly in Blood Serum. Anal. Chem 2007, 79, 229–233. [PubMed: 17194144]

(27). Lubin AA; Plaxco KW Folding-Based Electrochemical Biosensors: The Case for Responsive Nucleic Acid Architectures. Acc. Chem. Res 2010, 43, 496–505. [PubMed: 20201486]

(28). Ellington AD; Szostak JW In vitro selection of RNA molecules that bind specific ligands. Nature 1990, 346, 818–822. [PubMed: 1697402]

(29). Tuerk C; Gold L Systematic Evolution of Ligands by Exponential Enrichment: RNA Ligands to Bacteriophage T4 DNA Polymerase. Science 1990, 249, 505–510. [PubMed: 2200121]

(30). Feagin TA; Maganzini N; Soh HT Strategies for Creating Structure-Switching Aptamers. ACS Sens. 2018, 3, 1611–1615. [PubMed: 30156834]

(31). Oh SS; Plakos K; Lou X; Xiao Y; Soh HT In vitro selection of structure-switching, self-reporting aptamers. Proc. Natl. Acad. Sci. U.S.A 2010, 107, 14053–14058. [PubMed: 20660786]

(32). Ray P; Viles KD; Soule EE; Woodruff RS Application of Aptamers for Targeted Therapeutics. Arch. Immunol. Ther. Exp 2013, 61, 255–271.

(33). Tong P; Zhang L; Xu J-J; Chen H-Y Simply Amplified Electrochemical Aptasensor of Ochratoxin A Based on Exonuclease-Catalyzed Target Recycling. Biosens. Bioelectron 2011, 29, 97–101. [PubMed: 21855315]

(34). Wang C; Li Y; Zhao Q A Signal-on Electrochemical Aptasensor for Rapid Detection of Aflatoxin B1 Based on Competition with Complementary DNA. Biosens. Bioelectron 2019, 144, 111641. [PubMed: 31494505]

(35). Willner I; Zayats M Electronic Aptamer-Based Sensors. Angew. Chem., Int. Ed 2007, 46, 6408–6418.

(36). Plaxco KW; Soh HT Switch-Based Biosensors: A New Approach towards Real-Time, in Vivo Molecular Detection. Trends Biotechnol. 2011, 29, 1–5. [PubMed: 21106266]

(37). Wu L; Zhang X; Liu W; Xiong E; Chen J Sensitive Electrochemical Aptasensor by Coupling ″Signal-on" and ″Signal-off" Strategies. Anal. Chem 2013, 85, 8397–8402. [PubMed: 23998713]

(38). Zhao J; He X; Bo B; Liu X; Yin Y; Li GA ″signal-on″ electrochemical aptasensor for simultaneous detection of two tumor markers. Biosens. Bioelectron 2012, 34, 249–252. [PubMed: 22386488]

(39). Xiao Y; Piorek BD; Plaxco KW; Heeger AJ A Reagentless Signal-On Architecture for Electronic, Aptamer-Based Sensors via Target-Induced Strand Displacement. J. Am. Chem. Soc 2005, 127, 17990–17991. [PubMed: 16366535]

(40). Song S; Wang L; Li J; Fan C; Zhao J Aptamer-Based Biosensors. Trac. Trends Anal. Chem 2008, 27, 108–117.

(41). Zhao N; Pei S-N; Qi J; Zeng Z; Iyer SP; Lin P; Tung C-H; Zu Y Oligonucleotide Aptamer-Drug Conjugates for Targeted Therapy of Acute Myeloid Leukemia. Biomaterials 2015, 67, 42–51. [PubMed: 26204224]

(42). Jiang H; Zhou X; Kulkarni S; Uranian M; Seenivasan R; Hall DA A Sub-1 μW multiparameter injectable BioMote for continuous alcohol monitoring. In 2018 IEEE Custom Integrated Circuits Conference (CICC); IEEE, 2018; pp 1–4.

(43). Ferapontova EE; Olsen EM; Gothelf KV An RNA Aptamer-Based Electrochemical Biosensor for Detection of Theophyl-line in Serum. J. Am. Chem. Soc 2008, 130, 4256–4258. [PubMed: 18324816]

(44). Taguchi T; Sonobe H; Toyonaga S.-i.; Yamasaki I; Shuin T; Takano A; Araki K; Akimaru K; Yuri K Conventional and Molecular Cytogenetic Characterization of a New Human Cell Line, GIST-T1, Established from Gastrointestinal Stromal Tumor. Lab. Invest 2002, 82, 663–665. [PubMed: 12004007]

(45). Collie GW; Parkinson GN The Application of DNA and RNA G-Quadruplexes to Therapeutic Medicines. Chem. Soc. Rev 2011, 40, 5867–5892. [PubMed: 21789296]

(46). Tucker WO; Tanner KTS; J A G-quadruplex DNA Aptamers and their Ligands: Structure, Function and Application. http://www.eurekaselect.com/96329/article (accessed June 6, 2020).

(47). Radi A-E; O'Sullivan CK Aptamer Conformational Switch as Sensitive Electrochemical Biosensor for Potassium Ion Recognition. Chem. Commun 2006, 32, 3432–3434.

(48). Xiao Y; Lubin AA; Heeger AJ; Plaxco KW Label-Free Electronic Detection of Thrombin in Blood Serum by Using an Aptamer-Based Sensor. Angew. Chem 2005, 117, 5592–5595.

(49). Jo H; Kim S-K; Youn H; Lee H; Lee K; Jeong J; Mok J; Kim S-H; Park H-S; Ban C A Highly Sensitive and Selective Impedimetric Aptasensor for Interleukin-17 Receptor A. Biosens. Bioelectron 2016, 81, 80–86. [PubMed: 26921556]

(50). Kypr J; Kejnovská I; Renciuk D; Vorlícková M Circular Dichroism and Conformational Polymorphism of DNA. Nucleic Acids Res. 2009, 37, 1713–1725. [PubMed: 19190094]

(51). Cruz AC; Frank BT; Edwards ST; Dazin PF; Peschon JJ; Fang KC Tumor Necrosis Factor-α-converting Enzyme Controls Surface Expression of c-Kit and Survival of Embryonic Stem Cell-derived Mast Cells. J. Biol. Chem 2004, 279, 5612–5620. [PubMed: 14625290]

(52). Llovet JM; Peña CEA; Lathia CD; Shan M; Meinhardt G; Bruix J Plasma Biomarkers as Predictors of Outcome in Patients with Advanced Hepatocellular Carcinoma. Clin. Cancer Res 2012, 18, 2290–2300. [PubMed: 22374331]

(53). Singh N; Huang L; Wang D-B; Shao N; Zhang X-E Simultaneous Detection of a Cluster of Differentiation Markers on Leukemia-Derived Exosomes by Multiplex Immuno-Polymerase Chain Reaction via Capillary Electrophoresis Analysis. Anal. Chem 2020, 92, 10569–10577. [PubMed: 32600030]

(54). Ainsua-Enrich E; Serrano-Candelas E;Álvarez-Errico D; Picado C; Sayós J; Rivera J; Martín M The Adaptor 3BP2 Is Required for KIT Receptor Expression and Human Mast Cell Survival. J. Immunol 2015, 194, 4309–4318. [PubMed: 25810396]

(55). Tabone S; Théou N; Wozniak A; Saffroy R; Deville L; Julié C; Callard P; Lavergne-Slove A; Debiec-Rychter M; Lemoine A; Emile J-F KIT Overexpression and Amplification in Gastrointestinal Stromal Tumors (GISTs). Biochim. Biophys. Acta 2005, 1741, 165–172. [PubMed: 15869870]

(56). Andreadis D; Epivatianos A; Poulopoulos A; Nomikos A; Papazoglou G; Antoniades D; Barbatis C Detection of C-KIT (CD117) Molecule in Benign and Malignant Salivary Gland Tumours. Oral Oncol. 2006, 42, 56–64.

(57). Rassidakis GZ; Georgakis GV; Oyarzo M; Younes A; Medeiros LJ Lack of C-Kit (CD117) Expression in CD30+ Lymphomas and Lymphomatoid Papulosis. Mod. Pathol 2004, 17, 946–953. [PubMed: 15105813]

(58). Kwon H-S; Logan AC; Chhabra A; Pang WW; Czechowicz A; Tate K; Le A; Poyser J; Hollis R; Kelly BV; Kohn DB; Weissman IL; Prohaska SS; Shizuru JA Anti-Human CD117 Antibody-Mediated Bone Marrow Niche Clearance in Nonhuman Primates and Humanized NSG Mice. Blood 2019, 133, 2104–2108. [PubMed: 30617195]

(59). Srivastava M; Nirala NR; Srivastava SK; Prakash R A Comparative Study of Aptasensor Vs Immunosensor for Label-Free PSA Cancer Detection on GQDs-AuNRs Modified Screen-Printed Electrodes. Sci. Rep 2018, 8, 1923. [PubMed: 29386538]

(60). Ahirwar R; Dalal A; Sharma JG; Yadav BK; Nahar P; Kumar A; Kumar S An Aptasensor for Rapid and Sensitive Detection of Estrogen Receptor Alpha in Human Breast Cancer. Biotechnol. Bioeng 2019, 116, 227–233. [PubMed: 30132794]

(61). Bono P; Krause A; von Mehren M; Heinrich MC; Blanke CD; Dimitrijevic S; Demetri GD; Joensuu H Serum KIT and KIT Ligand Levels in Patients with Gastrointestinal Stromal Tumors Treated with Imatinib. Blood 2004, 103, 2929–2935. [PubMed: 15070666]

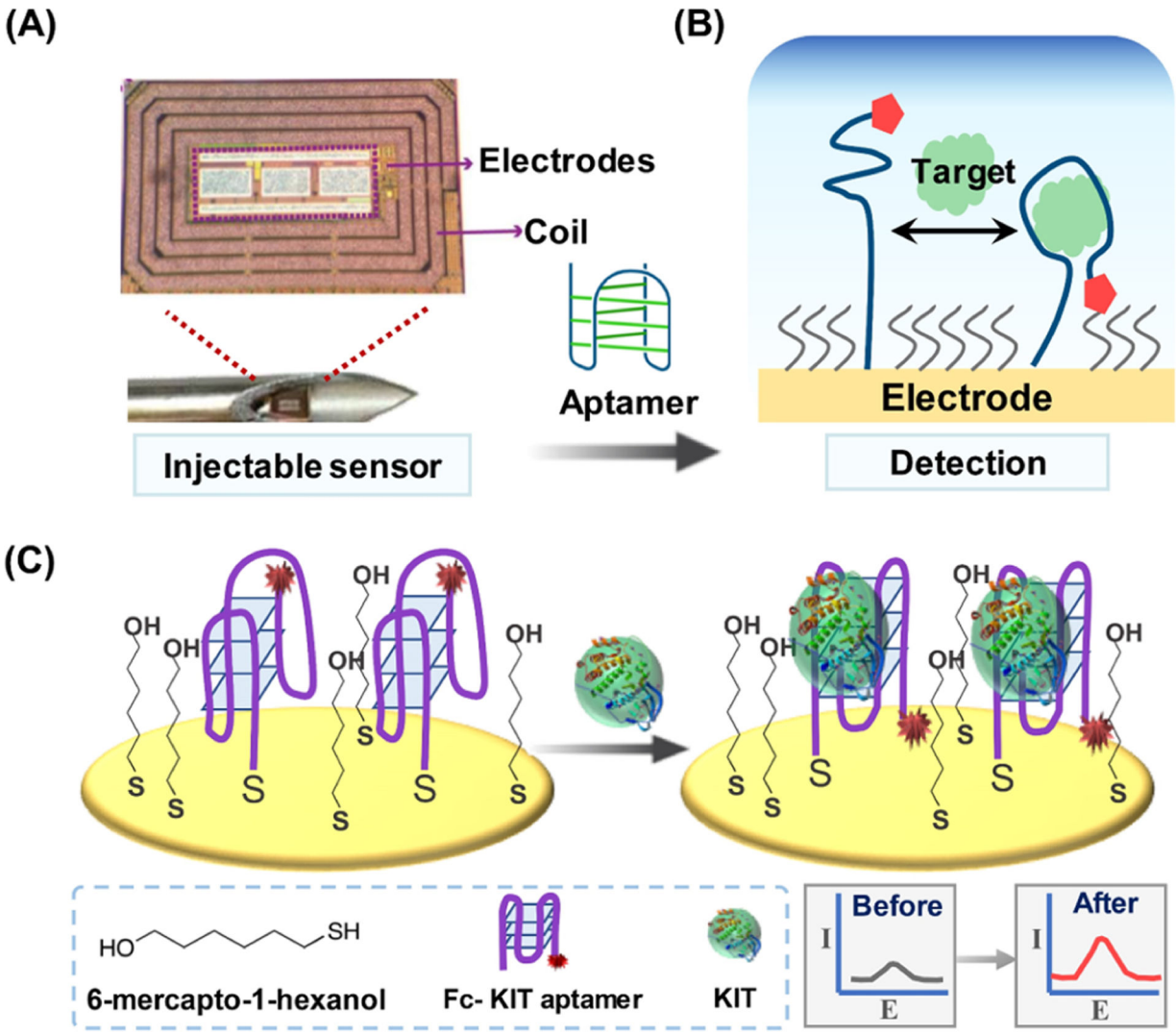

Figure 1.

Electrochemical KIT Aptasensor. (A) Vision of injectable sensor concept for continuous, *in vivo* cancer treatment monitoring. (B) Conformation switching aptasensor concept. (C) KIT aptamer with a Fc label in its unbound, unfolded state that modulates the Fc tag's position.

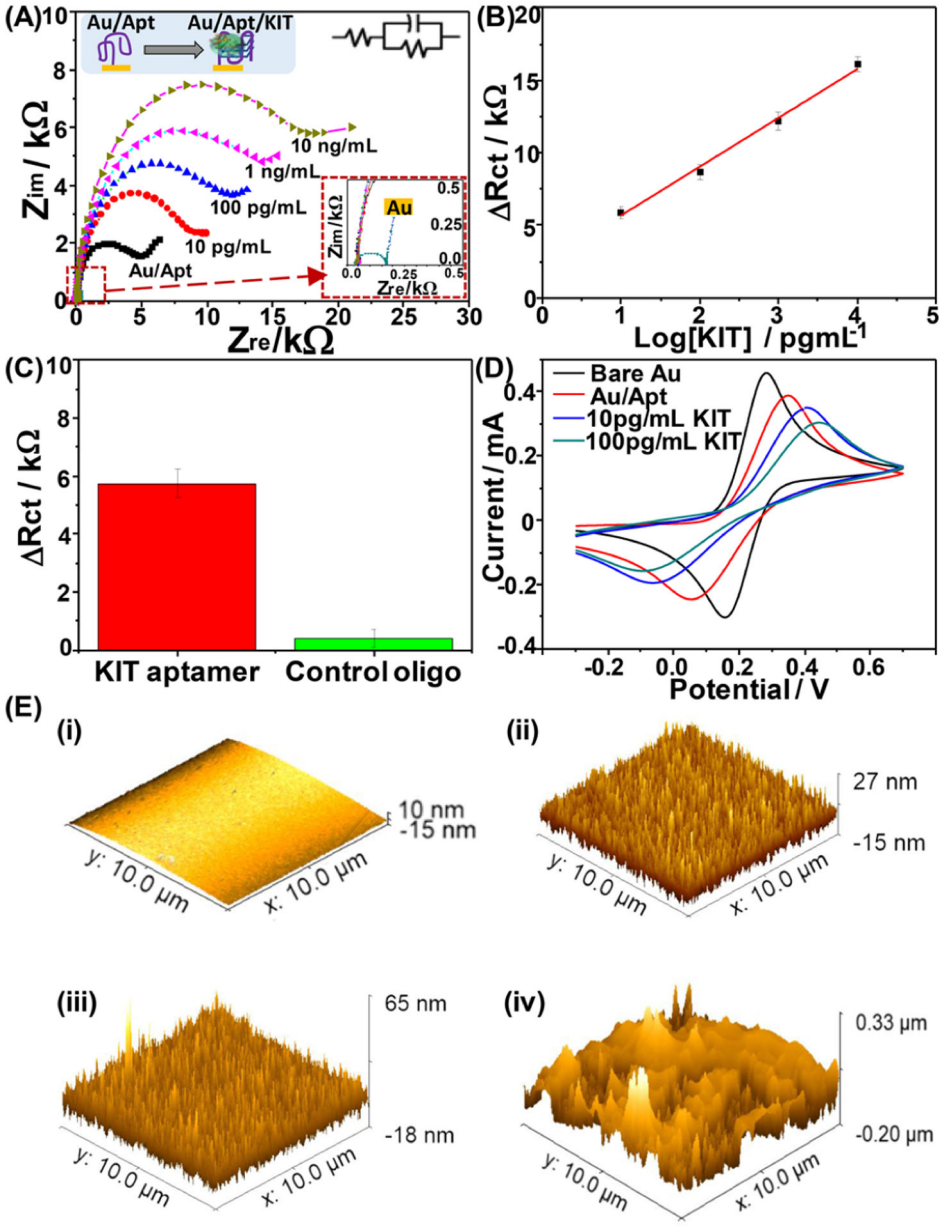

Figure 2.

Stepwise electrode assembly. (A) Nyquist plots of KIT aptasensor fabrication steps and spiked KIT protein in 5 mM $[Fe(CN)_6]^{4-/3-}$. (B) Extracted ΔR_{ct} vs log [KIT] with a linear fit. (C) Control experiment using the KIT aptamer and scrambled oligonucleotide-modified electrode with 10 pg/mL KIT protein. (D) Voltammograms of aptasensor fabrication in 5 mM $[Fe(CN)_6]^{4-/3-}$. All measurements were performed in triplicate, where error bars indicate $\pm 1\sigma$. (E) AFM images of (i) Au, (ii) Au/Apt, (iii) Au/Apt-Fc, and (iv) Au/Apt-Fc/KIT.

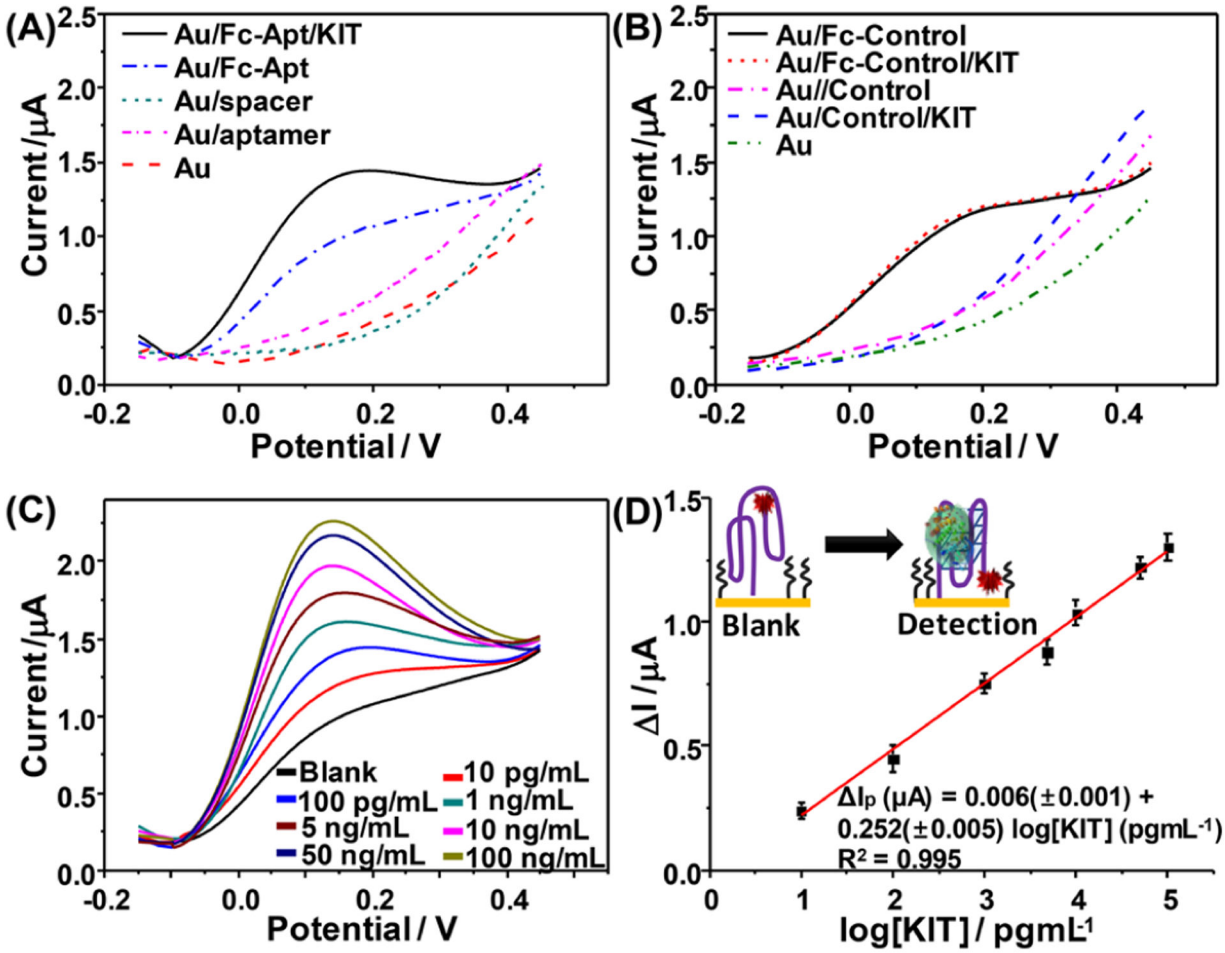

Figure 3.

Stepwise aptasensor assembly with Fc reporter and KIT detection. (A) Voltammograms of the KIT electrode. (B) Voltammograms of control oligo. (C) Voltammograms at various concentrations of KIT (10 pg/mL–100 ng/mL) in 0.1 M PBS (pH 7.4). (D) Calibration curve. All measurements were performed in triplicate, where error bars indicate ±1σ.

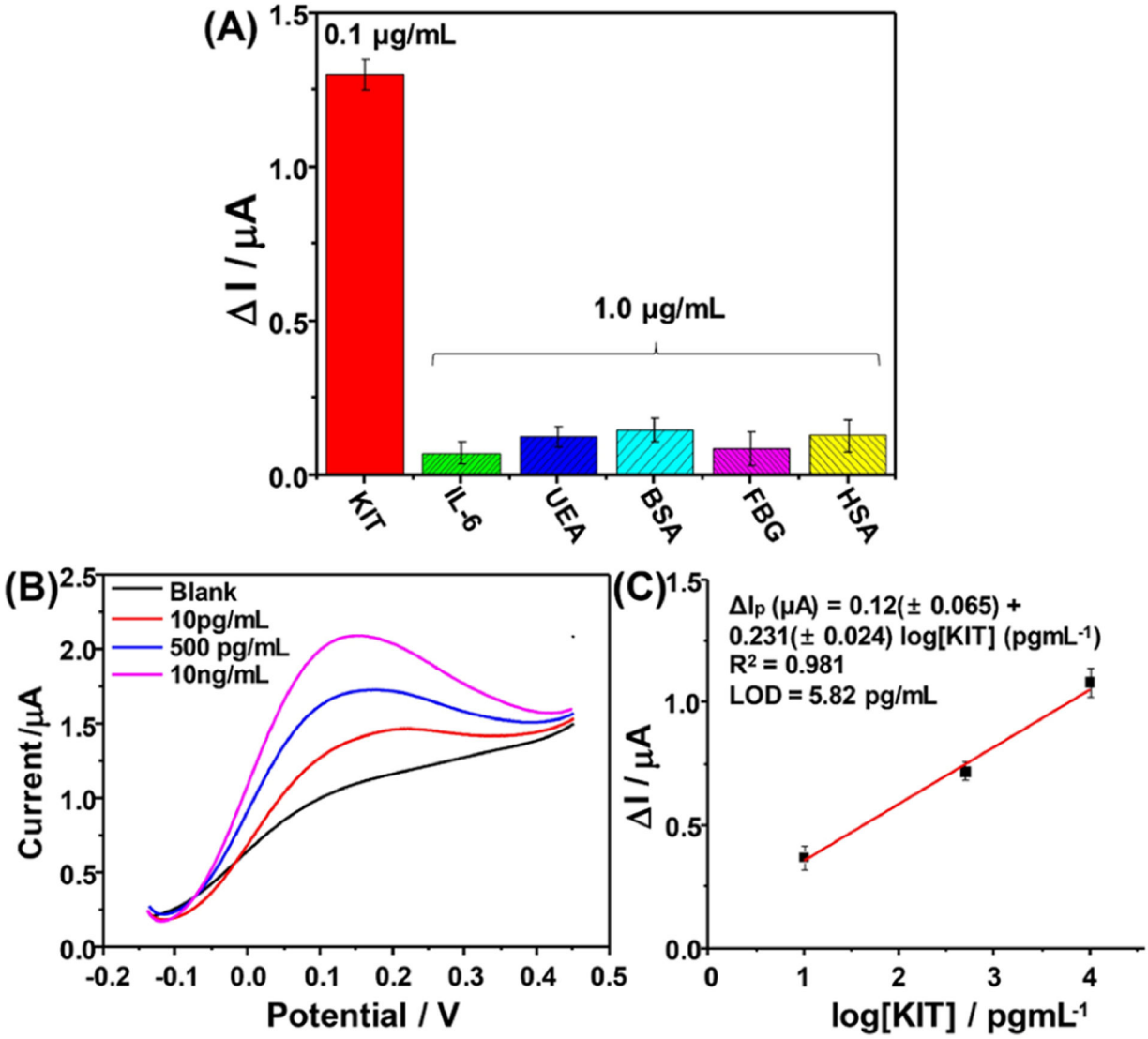

Figure 4.

Selectivity of the aptasensor. (A) Comparison of the aptasensor response to 0.1 μg/mL KIT and off-target proteins: IL-6, UEA, BSA, FBG, and HSA at 1 μg/mL. (B) Voltammograms recorded with spiked KIT in diluted human serum. (C) Calibration curve. All measurements were performed in triplicate, where error bars indicate $\pm 1\sigma$.

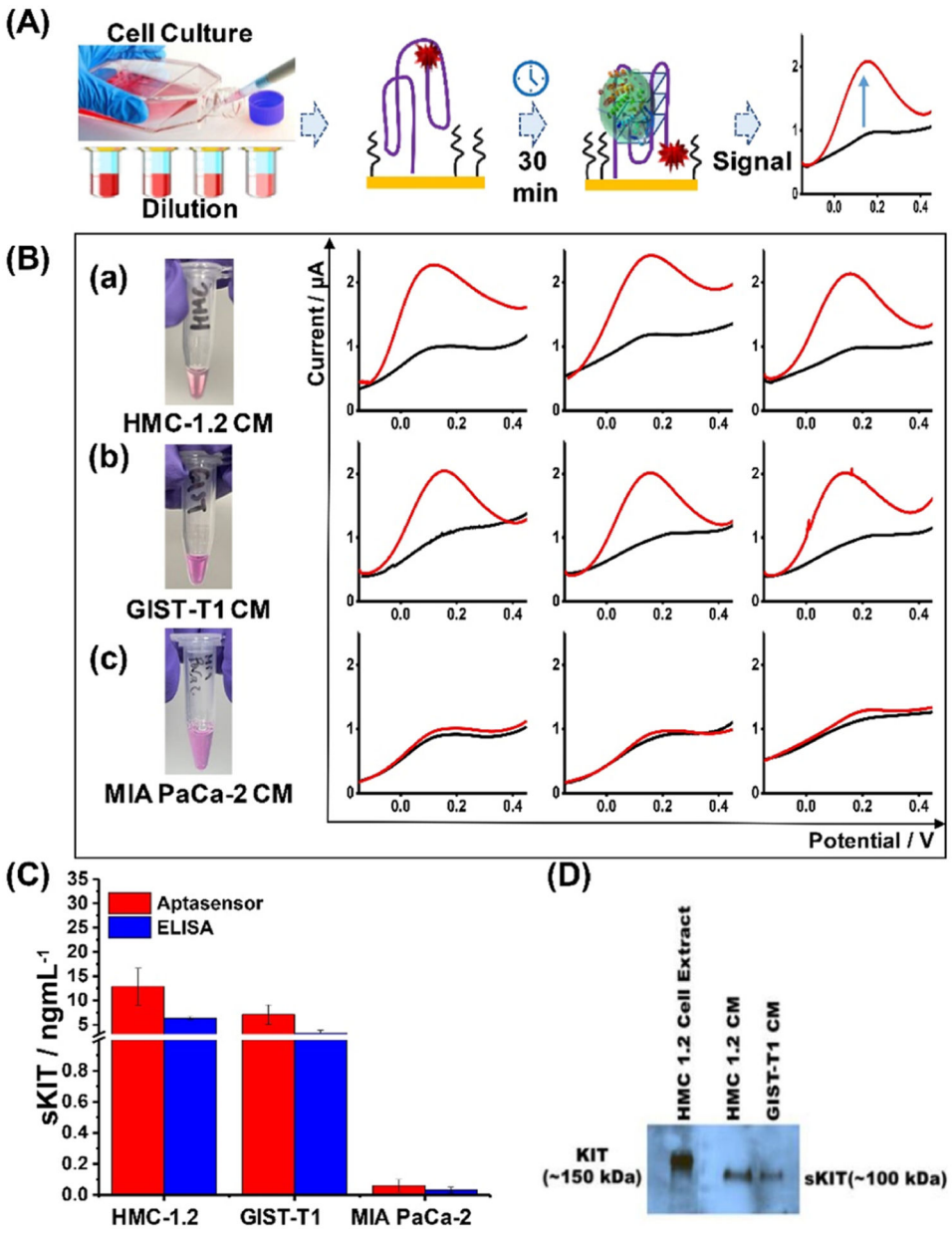

Figure 5.

Clinical applicability. (A) Schematic and (B) response of the KIT aptasensor 30 min after incubation using a conditioned medium of (a) HMC-1.2, (b) GIST-T1, and (c) MIA PaCa-2 cell lines. (C) Calculated sKIT concentration using aptasensor (red) and ELISA (blue) for each cell line. (D) Western blot assay results of sKIT in the conditioned media.

Table 1.

Comparison of Reported sKIT Detection Methods

method	receptor	detection limit (pg/mL)	dynamic range (ng/mL)	assay time (min)	*in vitro* or *in vivo?*
ELISA[51,52]	antibody	95	0.312–10	120	*in vitro*
	antibody	339	1.6–50	270	*in vitro*
immunohistochemical[56]	antibody			1500	*in vitro*
western blot[57]	antibody			1500	*in vitro*
flow cytometry[58]	antibody	5000		120	*in vitro*
mI-PCR[53]	antibody	2.41		150	*in vitro*
electrochemical aptasensor (this work)	**aptamer**	**1.15**	**0.010–100**	**35**	***in vivo* and *in vitro***